Controls on zircon age distributions in volcanic, porphyry and plutonic rocks

Chetan Nathwani[1], Dawid Szymanowski[1], Lorenzo Tavazzani[1], Sava Markovic[1], Adrianna L. Virmond[1], and Cyril Chelle-Michou[1]

[1]Institute of Geochemistry and Petrology, ETH Zürich, 8092 Zürich, Switzerland

Correspondence: Chetan Nathwani (chetan.nathwani@eaps.ethz.ch)

Abstract. The distribution of zircon crystallisation ages in igneous rocks has been proposed to provide insights into the dynamics of underlying magma reservoirs. However, the ability to interpret magmatic processes from an age distribution is challenged by a complex interplay of factors such as sampling biases, analytical uncertainties and incorporation of extraneous zircon grains. Here, we use a compilation of igneous zircon U-Pb ages measured by chemical abrasion isotope dilution thermal ionisation mass spectrometry (CA-ID-TIMS) to quantify the differences that exist among zircon U-Pb age distributions from different magmatic systems. The compiled dataset was rigorously filtered through a number of processing steps to isolate age distributions least impacted by sampling biases and analytical factors. We also filter the database using a new algorithm to systematically identify and remove old outliers from age distributions. We adopt the Wasserstein distance as a dissimilarity metric to quantify the difference between the shapes of age distributions. Principal component analysis (PCA) of a dissimilarity matrix of pairwise Wasserstein distances between age distributions reveals differences among zircon age distributions found in plutonic, porphyry and volcanic rocks. Volcanic and porphyry zircon populations exhibit a skew towards younger ages in their distributions, whereas plutonic age distributions skew towards older ages. We use a bootstrap forward modelling approach to generate synthetic zircon age distributions, which are cast into the PCA space of the dissimilarity matrix of natural age distributions to allow us to identify the magmatic processes which reproduce distributions found in natural data. We find that the younger skew of porphyry and volcanic zircon age distributions can be reproduced under bootstrap sampling scenarios where zircon crystallisation is truncated (e.g. by volcanic eruption or porphyry dyke emplacement). We also find that sampling underlying zircon age distributions generated under higher magmatic flux can contribute to the younger skew of volcanic and porphyry zircon age distributions, though we emphasise that no difference in flux is required due to the strong effect of truncation. Given the multitude of factors that influence observed zircon age distributions, we urge caution when quantifying the thermal evolution of crustal magma bodies using zircon age distributions integrated with numerical models.

1 Introduction

U–Th–Pb geochronology of zircon in igneous rocks provides key information about the age, longevity, and emplacement rates of magma reservoirs. Historically, the achievable age resolution limited these insights to a singular 'age', but as analytical precision and accuracy have improved, it has become possible to resolve extended records of zircon crystallisation within a

single igneous rock sample. These zircon crystals can predate the eruption or final solidification of a magma body by as much as a million years (Brown and Fletcher, 1999; Wotzlaw et al., 2013; Barboni et al., 2015; Samperton et al., 2015; Szymanowski et al., 2019). The observed zircon populations may result from cooling of the magma volume in which they are found (i.e. they are autocrystic, Wotzlaw et al., 2013; Samperton et al., 2015) or they could reflect the juxtaposition of zircon populations that derive from multiple depths within the crustal column (e.g., Schoene et al., 2012; Farina et al., 2018). While still relatively under-explored, distributions of zircon ages are promising recorders of processes that are critical to the ultimate fate of the host magmatic system (e.g. a volcanic eruption or economic mineralisation). In several studies, zircon age distributions have been shown to match those produced from zircon solubility models and thus have been interpreted as the product of monotonous cooling of the magmatic system (Samperton et al., 2017; Keller et al., 2018). Others have documented age distributions which differ from these zircon solubility models and have attributed this to competition between cooling and recharge of the magma reservoir which shifts the peak in the distribution to younger ages (Schmitt et al., 2023; Tavazzani et al., 2023a). Coupling of zircon age distributions with outputs from numerical models has been used to quantify magmatic fluxes (Caricchi et al., 2014, 2016; Weber et al., 2020; Liu et al., 2021; Schmitt et al., 2023) and to propose that greater fluxes exist in magma reservoirs forming super-eruptions compared to plutonic complexes (Caricchi et al., 2014).

Isolating the effect of cooling and recharge processes on zircon age distributions can be challenging since a number of analytical and geological factors may play a role (Klein and Eddy, 2023). Firstly, a key requirement of this comparison is the ability to confidently resolve differences in crystallisation age within a single rock sample, i.e., to ensure that the observed distribution is controlled by geological dispersion rather than analytical uncertainty. This ability, best described by the apparent duration of zircon crystallisation with respect to the size of average analytical uncertainties of a dataset ($\Delta t/\sigma$), varies with the employed analytical technique, the time range of zircon crystallisation and absolute age. Datasets also contain variable numbers of zircon dates per sample and the ability to accurately capture the underlying age distribution increases with the number of zircons analysed (Caricchi et al., 2016; Tavazzani et al., 2023a). Interpreting age distributions is further challenged by the termination of zircon crystallisation at intermediate crystallinity by dyke emplacement or volcanic eruption (a process we refer to herein as 'truncation'), whereas in plutonic systems zircon crystallisation likely continues until the solidus (Samperton et al., 2017; Ratschbacher et al., 2018). Comparing age distributions is also complicated due to the challenge in identifying whether these zircons crystallised from the youngest magmatic pulse (i.e. 'autocrysts') or are a cargo of zircons crystallised in multiple, discrete systems that were incorporated upon transport ('antecrysts') (Miller et al., 2007).

As the geochronology community presents a growing number of zircon age distributions from different magmatic systems with sufficiently long duration to analytically resolve an age distribution, constraining the controls on their distributions is becoming increasingly relevant. The number of available datasets has now become sufficient to perform systematic analyses of published data to identify patterns that can be meaningfully attributed to geological processes. Such a comparison requires a robust statistical approach which is capable of comparing distributions with varying dataset size and analytical uncertainty without making assumptions about the shape of the distribution. The use of dissimilarity metrics, such as the Kolmogorov-Smirnov and Wasserstein distances, is becoming increasingly popular to compare age distributions, with successful applications to tracing sediment provenance in multi-sample datasets (Vermeesch, 2013; Lipp and Vermeesch, 2023). These approaches

Table 1. Symbols used in this study and their definitions

Symbol	Definition
Δt	Absolute duration of zircon crystallisation
Δt_{rel}	Time between two zircon crystallisation distributions
t_i	Time of crystallisation of ith zircon
t_{rel}	Relative time of zircon crystallisation
t_{sat}	Time of initial zircon saturation
t_{end}	Time of termination of zircon crystallisation
σ	Uncertainty
ECDF	Empirical cumulative distribution function
KDE	Kernel density estimation
$\hat{F}_n(t)$	Interpolated ECDF of t
f_{xtal}	Zircon age probability density function
W_p	The pth Wasserstein distance
n_{zircon}	Number of zircon crystals
n_{inh}	Number of inherited zircon crystals
δ	Delta function
d	Dissimilarity matrix
w_i	Weighting of i
$\nabla\hat{F}_n(t)$	Gradient of interpolated ECDF
∇_M	Gradient below which an ECDF is marked as discontinuous
t_{flat}	Relative time of ECDF below
M^{-1}	Inverse function of M

60   are objective and they can be applied pairwise to datasets with infinite numbers of distributions and can be visualised using dimensionality reduction techniques (Vermeesch, 2013).

In this study, we compare zircon age spectra from 70 igneous units using the Wasserstein dissimilarity metric to constrain whether differences in age spectra may reflect variable dynamics of magmatic systems. We identify key differences between age distributions in plutonic, volcanic and porphyry lithologies and use a bootstrap modelling approach to explore the key

65   factors controlling the variability of zircon age distributions in magmatic systems.

2 Methodology

2.1 Zircon U-Th-Pb age spectra and their visualisation

The high precision allowed by state-of-the-art U-Th-Pb dating techniques is showcased in rank-order plots of zircon dates from a single sample (Fig. 1A). In this scenario, zircon dates exhibit dispersion between the onset of zircon crystallisation (i.e. initial zircon saturation, t_{sat}) and the end of zircon crystallisation (t_{end}), which represents an eruptive event or the final solidification of a magma batch. These are often treated as a scaled relative zircon crystallisation distribution, $f_{xtal}(t_{rel})$, where t_{rel} is the relative time scaled between t_{sat} and t_{end} (Keller et al., 2018):

$$t_{rel} = \frac{t - t_{end}}{t_{sat} - t_{end}} \tag{1}$$

The $f_{xtal}(t_{rel})$ of a sample can be visualised as a kernel density estimate (KDE; Fig. 1B) which is where a series of kernels (typically Gaussian) of a fixed width (the "bandwidth") are stacked along the distribution (Vermeesch, 2012). The main advantage of KDE plots is their ability to represent the distribution of zircon dates in an intuitive manner, moreover, they can be weighted by the variable analytical uncertainties associated to each zircon date. Another method for visualising such age distributions is an empirical cumulative distribution function (ECDF; Fig. 1C), which is a step function that increases by $1/n$ (or by an interval inverse to the analytical uncertainty) at each of the n dates. The ECDF, though less intuitive, presents several advantages. The first is that outliers (e.g. xenocrysts) can be more easily identified because it is a step function that plots each discrete date unlike a KDE plot. The second is that it can be more intuitively related to dissimilarity metrics (e.g. the Kolmogorov–Smirnov test and the Wasserstein distance) which are related to the distances between two ECDFs. We thus henceforth prefer to visualise age distributions as ECDFs.

2.2 Filtering of outliers in age distributions

The biggest obstacle to identifying a truly "magmatic" age distribution is the presence of entire zircons or zircon domains (e.g. crystal cores) which are foreign to the youngest magmatic pulse, introduced into the magma via assimilation/mixing during emplacement or transport. Zircon crystals that formed within the youngest magmatic pulse are typically defined as "autocrysts", and those that crystallise in an earlier magmatic pulse related to older pulses of the composite, longer-term magmatic system are often termed "antecrysts" (Miller et al., 2007). "Xenocrysts" are those incorporated from host rocks and are typically millions of years older, which makes them easier to exclude than antecrysts.

When analysing datasets of concordant U-Pb dates, identifying antecrysts in an age distribution is subjective. Many recent interpretations of zircon age–composition datasets acknowledge that zircon populations found in individual igneous rocks commonly represent crystallisation in complex magmatic plumbing systems (e.g. Szymanowski et al., 2019; Pamukçu et al., 2022), thereby making the autocryst–antecryst divide ambiguous, and possibly detrimental to the understanding of the underlying system. Some authors may decide to exclude older tails of age distributions from their interpretation, but the criteria to do so are variable and often not clearly outlined. In some studies this can be based on different trace element compositions of older
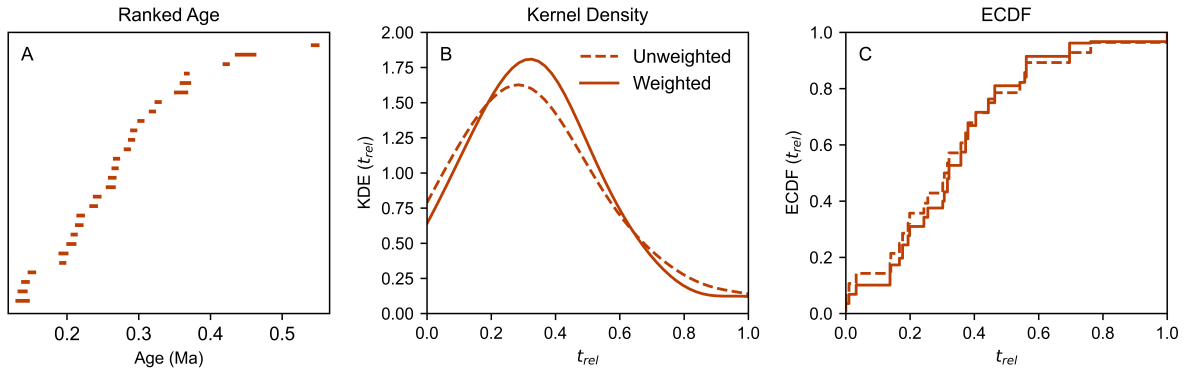
Figure 1. A comparison of three visualisation approaches employed in geochronology using an example zircon U-Pb ID-TIMS dataset from the Youngest Toba Tuff (Szymanowski et al., 2023). (A) Ranked age plot (youngest to oldest) where the horizontal extent of the bars indicates the 2σ uncertainty on each U-Pb date. (B) Kernel density estimate (KDE) using both unweighted (dashed) and weighted (solid) estimates and, (C) weighted (dashed) and unweighted (solid) empirical cumulative distribution frequency (ECDF) curves, both scaled between onset and end of zircon crystallisation (t_{rel}).

zircon, inferring they were derived from an unrelated magmatic pulse (e.g., Gagnevin et al., 2010; Siégel et al., 2018; Tavazzani et al., 2023a). Other studies may also use "breaks" in the age distribution to indicate that the older zircon crystals were derived from a different source (e.g., Samperton et al., 2015).

100   In this study, we present a method to filter old outliers from age distributions using constant criteria. The algorithm removes older outlier dates from an age distribution which are separated from the rest of the dataset by a fixed relative time gap. Because old outliers introduce low gradient regions on an ECDF (e.g. black curve on Fig. 2), we identify potential antecrysts based on the gradient of an ECDF (Fig. 1C). The model first calculates the gradient of an ECDF, where $\hat{F}_n(t_{rel})$ is the interpolated ECDF:

$$105 \quad \nabla\hat{F}_n(t_{rel}) = \frac{\mathrm{d}\hat{F}_n(t_{rel})}{\mathrm{d}t_{rel}} \tag{2}$$

A gradient cut-off term (∇_M) is then defined, that represents the gradient below which a segment of an ECDF will be defined as marking a discontinuity in the age distribution (Fig. 2). For a scaled age distribution, we then sum the length of the flat segments of the ECDF older than the two youngest dates (to ignore age gaps at the young end of the distribution which are not considered here):

$$110 \quad t_{flat} = \sum_{i=3}^{n_{zircon}-1} \begin{cases} t_{i+1} - t_i & \text{if } \nabla\hat{F}_n(t_i) < \nabla_M \\ 0 & \text{otherwise.} \end{cases} \tag{3}$$

    This metric t_{flat} then provides a quantification of the scaled age duration that is not continuously covered with U-Pb dates (Fig. 2). For age distributions with two discontinuous age populations, t_{flat} will scale with increasing temporal distance

between the two populations. The choice of t_{flat} that is deemed acceptable ($t_{flat_{max}}$) for such an age distribution is subjective (i.e. at a low t_{flat} the two age populations will be considered continuous).

If an age distribution yields $t_{flat} < t_{flat_{max}}$ it is deemed to come from one continuous age population. In the opposite case (i.e. $t_{flat} > t_{flat_{max}}$), the oldest date is iteratively removed until a continuous age population ($t_{flat} < t_{flat_{max}}$) is obtained. The two parameters ∇_M and $t_{flat_{max}}$ were tuned until the filtering method was satisfactory in discarding significantly older zircons throughout the data compilation and did not filter those which were potentially part of the main age population. The optimal parameters determined for ∇_M and $t_{flat_{max}}$ are 0.30 and 0.25, respectively. Our method has functionality to perform filtering on weighted ECDFs (i.e. taking into account analytical uncertainty) but we did not implement it as it proved challenging to select constant parameters that would filter all datasets to an acceptable degree. We emphasise that our approach does not aim to provide a geologically significant method to isolate autocrystic zircons (which is impossible to verify), but rather a systematic method of isolating the dominant, continuous population (corresponding to the main magmatic pulse) across multiple datasets.

2.3 Igneous zircon geochronology compilation

Making interpretations about the dynamics of magma reservoirs from zircon age distributions requires confidence that the dispersion exhibited by the dataset is predominantly geological rather than analytical. One requirement is a sufficiently long duration of zircon crystallisation in a sample relative to the average analytical uncertainty ($\Delta t/\sigma$, as used by Keller et al., 2018). A high $\Delta t/\sigma$ allows the shape of a distribution to be deconvolved from analytical uncertainties, whereas low $\Delta t/\sigma$ age distributions are dominated by analytical uncertainty. Sufficient $\Delta t/\sigma$ in individual magmatic systems is generally only achieved by two analytical techniques: ^{230}Th–^{238}U disequilibrium dating applied to young zircon (predominantly obtained with *in situ* methods such as secondary ion mass spectrometry – SIMS or laser ablation inductively coupled plasma mass spectrometry – LA-ICP-MS) and high-precision U–Pb geochronology by (chemical abrasion) isotope dilution thermal ionisation mass spectrometry – (CA-)ID-TIMS (Schaltegger et al., 2015). The ^{230}Th–^{238}U method achieves variable, per cent-level precision which may be sufficient to resolve age distributions in the young rocks it is best suited to (< ca. 300 ka; Schmitt, 2011). However, difficulty in calculating reliable individual zircon model ages in the absence of a matching coeval melt or other mineral phase, the effective upper age limit of *ca.* 300 ka, and a focus of existing datasets on volcanic rocks limit the utility of ^{230}Th–^{238}U data for our study. On the other hand, CA-ID-TIMS U–Pb geochronology is applied to zircons from *ca.* 100 ka to the age of the Solar System, achieves a typical precision of ^{206}Pb/^{238}U dates between 0.01–1%, and is widely applied to plutonic, subvolcanic (i.e. porphyry) and volcanic zircon (Schoene, 2014). Given that the resolving power of U–Pb geochronology decreases with increasing age, we focused our analysis exclusively on CA-ID-TIMS data for the ^{206}Pb/^{238}U chronometer most applicable to young (<1 Ga) rocks.

In order to systematically compare zircon age distributions between different magmatic systems, we adopted a previously compiled database of published zircon U-Pb dates (Markovic et al., 2024). We classified and sub-selected data from samples clearly identifiable as either plutonic, porphyry, or proximal volcanic deposits. This permits a comparison of age distributions in a diverse range of igneous rocks. We excluded distal volcanic materials such as ash beds or bentonites to avoid biases related to transport sorting or included detrital material. While complete exclusion of cases of Pb loss is not verifiable, we focused
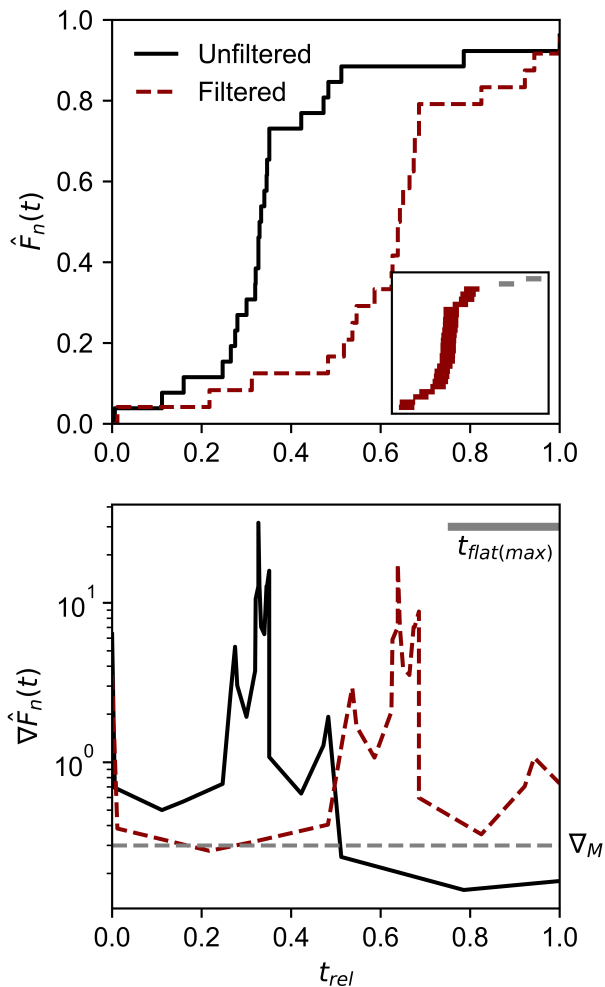
Figure 2. An example of the methodology used to filter older age populations from the age distribution of a sample from the Orano dyke swarm, Elba island (Barboni et al., 2015). Upper plot shows the weighted ECDF of the age distribution before and after the filtering process. Inset diagram shows the ranked age plot (not scaled by the uncertainty), with gray bars highlighting the two dates that were filtered by the method (uncertainties are not shown). Lower plot shows the gradient of the ECDF ($\nabla \hat{F}_n(t)$) before and after filtering. The dashed horizontal grey line indicates the gradient cut-off (∇_M) below which some degree of inheritance is deemed to have taken place, if the distance in scaled age is greater than the threshold ($t_{flat_{max}}$).

our analysis on samples least affected by radiation damage, only considering datasets with age $<$130 Ma. Rare cases of clear young outliers remaining in the database were excluded manually.

We only include age distributions with an apparent $\Delta t/\sigma$ greater than 10 to provide confidence that the age distribution is
150   sufficiently dispersed to isolate geological dispersion from analytical dispersion. Resolving an age distribution also requires a sufficient number of dates (n_{zircon}) from a magmatic unit. Many studies often report a small number of dates (e.g. five

Table 2. Sources of data used in the filtered zircon ID-TIMS U–Pb database and metadata describing the type of magmatic emplacement (plutonic, volcanic or porphyry), the mean 1σ analytical precision and the number of spectra present in the database for each locality.

Locality	Type	Mean Apparent Δt (Ma)	Mean Apparent $\Delta t/\sigma$	$n_{spectra}$	Reference
Adamello	Plutonic	0.35	14.0	1	Schoene et al. (2012)
Agua de Dionisio	Volcanic	0.13	17.9	1	Buret et al. (2017)
Bajo de la Alumbrera	Porphyry	0.16	15.3	3	Buret et al. (2016)
Batu Hijau	Porphyry	0.21	16.4	3	Large et al. (2020)
Bear Valley	Plutonic	0.58	14.4	3	Klein et al. (2021)
Bergell[1]	Plutonic	0.55	36.7	7	Samperton et al. (2015)
Bingham Canyon	Porphyry	0.39	37.7	2	Large et al. (2021)
Capanne[1]	Plutonic	0.31	80.6	6	Barboni et al. (2015)
Carpathian-Pannonian	Volcanic	0.46	40.1	3	Brlek et al. (2023)
Chegem	Volcanic	0.08	41.9	1	Bindeman et al. (2021)
Chuquicamata	Porphyry	0.73	27.2	8	Virmond et al. (2024)
Long Valley	Volcanic	0.03	10.0	1	Ickert et al. (2015)
Mogollon-Datil	Volcanic, Plutonic	0.72	28.3	6	Rioux et al. (2016); Szymanowski et al. (2019); Gaynor et al. (2023)
New England	Plutonic	2.45	37.8	2	Kinney et al. (2021)
Ok Tedi	Porphyry, Plutonic	0.12	11.7	3	Large et al. (2018)
Radomiro Tomic	Porphyry	1.19	44.2	4	Virmond et al. (2024)
Searchlight	Plutonic	0.16	10.9	1	Eddy et al. (2022)
Southern Rocky Mtns	Volcanic	0.99	22.4	5	Wotzlaw et al. (2013); Curry et al. (2021)
Spence	Porphyry	0.80	13.8	4	Bunker (2020)
Toba	Volcanic	0.27	84.3	4	Szymanowski et al. (2023)
Turkey Creek	Volcanic	0.30	16.7	1	Deering et al. (2016)
Yellowstone	Volcanic	0.10	10.9	1	Wotzlaw et al. (2015)

Age distributions contain sub-grain analyses[1]

or less), and in such scenarios the underlying age distribution is likely undersampled. The final dataset was thus limited to include only inheritance-filtered distributions that contained a minimum of 10 dates, as previous works indicate that sampling with less than 10 zircon dates fails to capture the underlying distribution (Klein and Eddy, 2023; Tavazzani et al., 2023b). We additionally found that some age distributions contain dates with highly variable analytical uncertainties, with some containing over an order of magnitude variation in uncertainties for zircon crystals dated from the same rock. Individual dates with high uncertainty in an age distribution impact the ability to resolve geological dispersion and in many cases would not be filtered using the apparent $\Delta t/\sigma$. We therefore calculate the weighting w that each date i holds in an age distribution using the inverse squared uncertainty (McLean et al., 2011):

$$w_i = \frac{\frac{1}{\sigma_i^2}}{\sum_{i=1}^{n_{zircon}} \frac{1}{\sigma_i^2}} \tag{4}$$

Age distributions with a standard deviation of w_i exceeding 0.08 were discarded. The final, filtered compilation contained 70 U-Pb age distributions from 22 magmatic systems (Fig. 3, Fig. S1, Table 2 and Table S1).
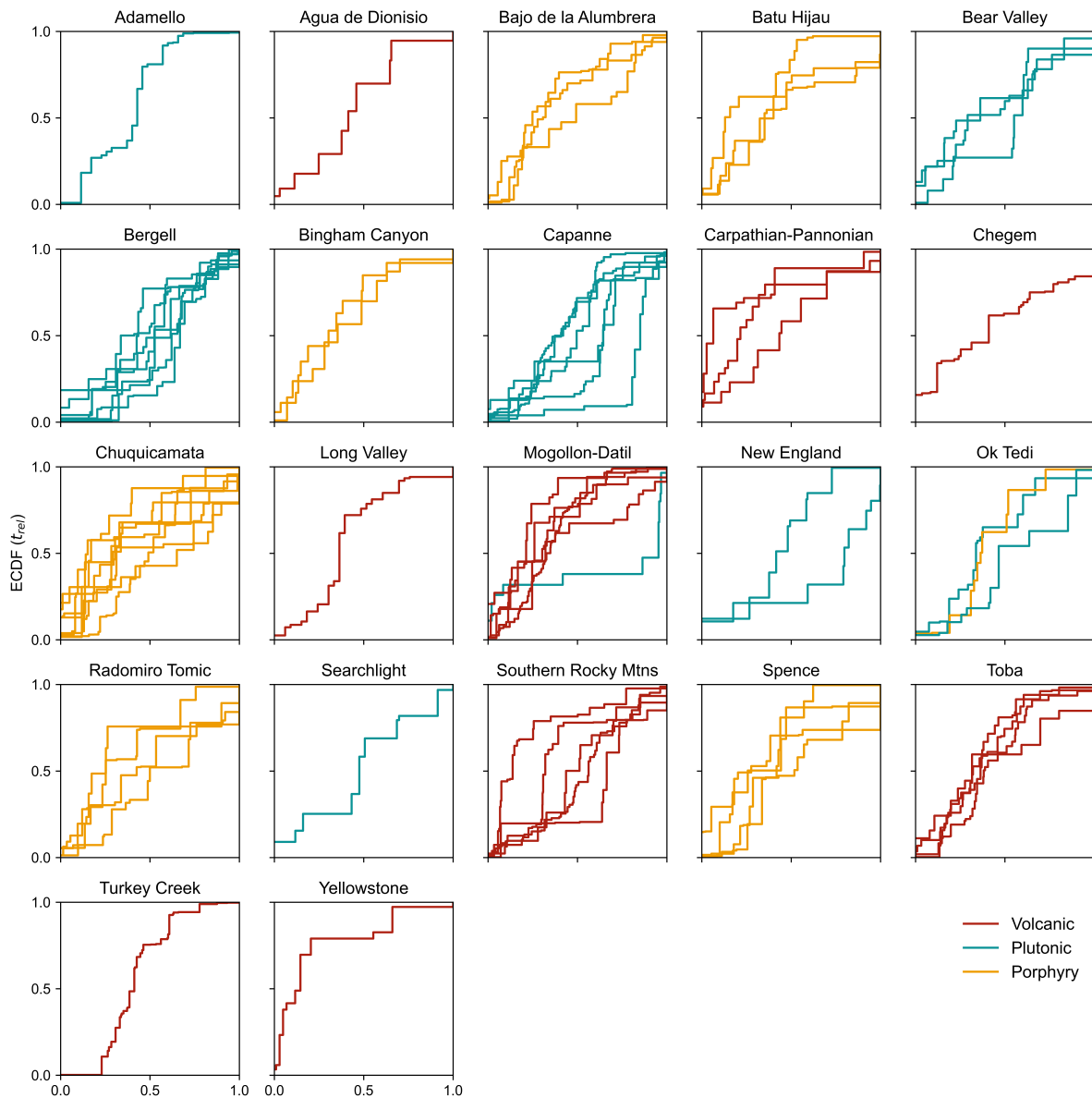
Figure 3. Weighted empirical cumulative distribution frequency curves for all 70 filtered zircon age distributions used in this study. Plots are separated based on the locality and curves indicate individual geological units within the locality. The color of each curve reflects the sample classification as volcanic (blue), plutonic (red) and porphyry (yellow) in the database.

2.4 The Wasserstein distance

The Wasserstein distance arises from the field of optimal transport and is a metric that allows comparison of two probability distributions. The metric is often termed the "earth mover's distance" because each probability distribution can be treated as a mound of earth, where the minimum cost of transferring earth from one mound to the other is the amount of earth multiplied by the distance it must be moved (Monge, 1781). Thus, the Wasserstein distance seeks to find the most efficient transport plan, which is the minimum cost of transporting one distribution to another. The optimal transport plan between two distributions is a measure of the dissimilarity of two distributions, with more dissimilar distributions requiring a greater cost and resulting in a larger Wasserstein distance. For two age distributions, μ and ν, with cumulative distribution functions (CDFs) M and N, the pth Wasserstein distance between them is given as:

$$W_p(\mu, \nu) = \left(\int_0^1 \left| M^{-1} - N^{-1} \right|^p dt \right)^{\frac{1}{p}} \tag{5}$$

The W_1 distance (i.e. where $p = 1$) is equal to the area between two ECDFs (Fig. 4). However, we follow the approach of Lipp and Vermeesch (2023) and implement the Wasserstein-2 distance (W_2) which is the squared distance ($p = 2$) and is akin to the standard distance metric used in most statistical analyses. The Python package *Python Optimal Transport* (v. 0.9.4 Flamary et al., 2021) is used for all optimal transport computations.

Zircon age datasets are discrete data and do not follow a continuous probability distribution and, as such, the Wasserstein distance applies to their empirical cumulative distribution frequency (ECDF) functions. In the case of ID-TIMS datasets, each date is not expected to hold equal weight due to variable analytical uncertainties. Thus the probability distributions μ and ν, can be represented as the weighted sum of p and q delta functions δ (Lipp and Vermeesch, 2023):

$$\mu = \sum_i^p m_i \delta_{x_m}, \nu = \sum_i^q n_i \delta_{x_n} \tag{6}$$

where *m* and *n* are weights that sum to 1. In the case where dates do not hold equal weight in the overall distribution, weights *m* and *n* can be calculated using Equation 4. We plot ECDFs and calculate the W_2 distance using the weights, and provide the same results calculated without weights for comparison (Figs. S2 and S3).

The Wasserstein distance has several advantages as a metric to compare zircon age distributions. In addition to allowing weighting based on uncertainty, it can be used on discrete ages (i.e. an ECDF) and does not require the inference of a specific prior distribution. The W_2 is also attractive in that, for two age distributions it is sensitive to their location (their means), spread (their standard deviations) and the shape of the distribution (Irpino and Romano, 2007; Lipp and Vermeesch, 2023). All three of these properties are relevant when considering two U-Pb age distributions. We prefer the Wasserstein distance to the Kolmogorov-Smirnov distance because the latter is a measure of the maximum vertical difference between the two ECDF and is, as such, less sensitive to the overall shape of the distribution.
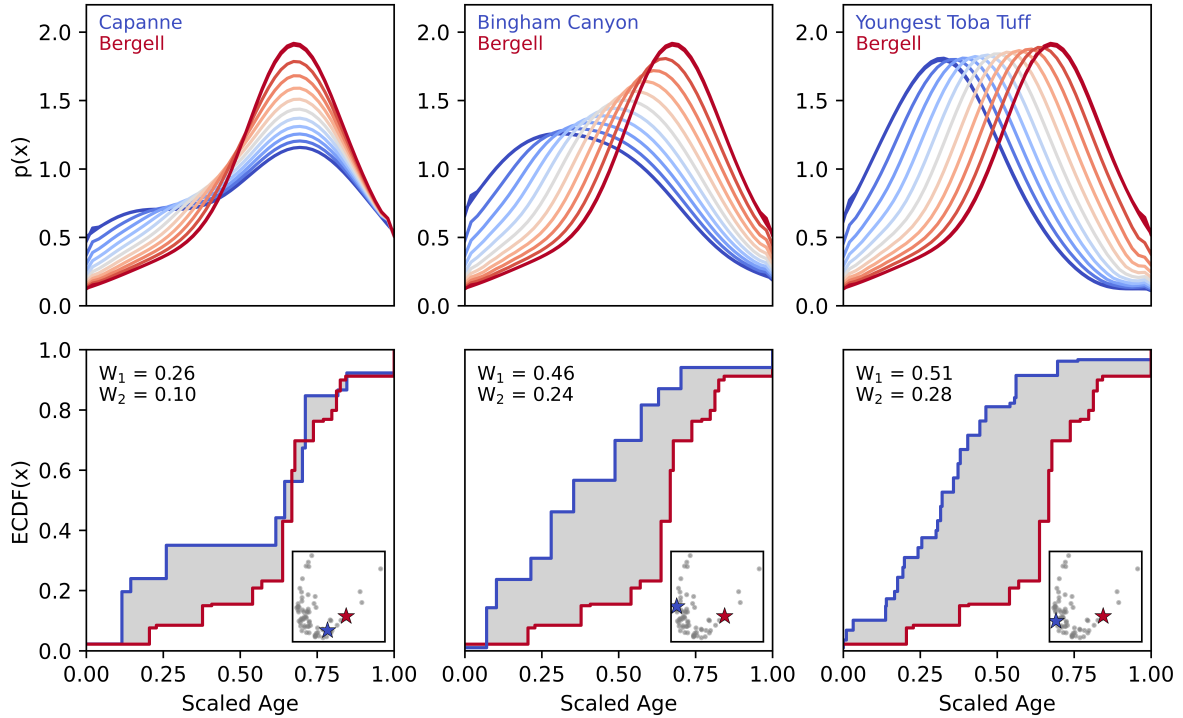
Figure 4. Examples showing three comparisons of similar to contrasting U-Pb ID-TIMS age distributions. Top row shows the distributions in blue and red with the transition distributions showing equally spaced (at 0.1 intervals) distributions in Wasserstein space (i.e. the Wasserstein barycentres). Bottom row shows the same two distributions as above as weighted ECDF curves, where the grey shaded area indicates the W_1 distance between the two distributions. The W_2 is also reported. Insets show where the two compared distributions plot on the PC1 versus PC2 diagram of the W_2 dissimilarity matrix (Fig. 5; see Section 2.5 for description of dissimilarity matrix construction).

2.5 Dissimilarity matrix and dimensionality reduction

The W_2 metric permits pairwise comparisons of age distributions. Thus for Y age distributions, a symmetric dissimilarity matrix, d of dimension $Y \times Y$ can be constructed:

$$d = \begin{bmatrix} d_{1,1} & d_{1,2} & \cdots & d_{1,Y} \\ d_{2,1} & d_{2,2} & \cdots & d_{2,Y} \\ \vdots & \vdots & \ddots & \vdots \\ d_{Y,1} & d_{Y,2} & \cdots & d_{Y,Y} \end{bmatrix} \tag{7}$$

Because the W_2 distance is a metric (i.e. it satisfies the triangle inequality), principal component analysis (PCA) can be applied to reduce the dissimilarity matrix to fewer dimensions whilst preserving the pairwise distances (Vermeesch, 2013; Lipp

and Vermeesch, 2023). PCA aims to preserve the variance of a dataset in a lower dimension space, where for a dissimilarity matrix this reflects the pairwise distances. We use the Python implementation within *sci-kit learn* (v. 1.5.1 Pedregosa et al., 2011) for PCA. The first two principal components contain 90% of the variance of the dissimilarity matrix, indicating that the majority of the pairwise distances are preserved with only 10% being lost.

2.6 Modelling approach

2.6.1 Bootstrap forward modelling of zircon age distributions

Forward modelling of synthetic age distributions and comparison with natural data can yield insights into the controls on age distributions in magmatic systems (Caricchi et al., 2014; Schmitt et al., 2023; Tavazzani et al., 2023a). This process aims to sample an underlying zircon age distribution according to realistic uncertainties and numbers of zircons sampled for ID-TIMS datasets. The underlying distribution, or the uncertainties and number of zircons sampled can be varied to test different hypotheses on the controls on zircon age distributions.

We follow the boostrap modelling approach of Tavazzani et al. (2023b). The model samples n_{zircon} synthetic dates from a probability distribution $p(x)$ which is equivalent to a selected underlying age distribution, such as the theoretical zircon age distribution obtained from zircon solubility and thermodynamic modelling of a monotonically cooling magma reservoir (Keller et al., 2018). For simplicity, our model assumes each zircon crystallises instantaneously and does not take into account the protracted growth of each individual zircon and the inherent volumetric bias of bulk grain analyses towards younger ages (Klein and Eddy, 2023). Gaussian uncertainty is then added to each synthetic age to reproduce uncertainties reported in ID-TIMS datasets. To calculate the uncertainty at a given age, we parametrised the reported 2σ absolute analytical uncertainty in the ID-TIMS compilation of Markovic et al. (2024) as a function of ^{206}Pb/^{238}U age (*t* in Ma) up to 1000 Ma using a second order polynomial fit. The resulting best fit parameters and covariance matrix yields the following equation with errors given as 2*SE*:

$$2\sigma = 5.5 \times 10^{-7}(\pm 2.8 \times 10^{-7})t^2 + 8.9 \times 10^{-4}(\pm 2.0 \times 10^{-4})t + 0.040(\pm 0.0162) \tag{8}$$

Gaussian uncertainty is propagated onto each date sampled during boostrap sampling according to the standard error on the fit parameters. The bootstrap sampling can be repeated with varying numbers of zircon grains, different age (and thus different analytical uncertainties) and with a different underlying distribution. These distributions can then be concatenated with the W_2 dissimilarity matrix generated on natural data. The pairwise dissimilarities of a modelled distribution with all natural distributions can then be transformed by PCA and visualised alongside natural data.

2.6.2 Magma recharge and underlying age distributions

The underlying age distribution from which zircon U-Pb dates are sampled can vary as a function of magmatic flux and volume (Caricchi et al., 2014; Tavazzani et al., 2023a). Keller et al. (2018) showed a remarkable similarity between age

distributions predicted from zircon solubility and thermodynamic models (Watson, 1996) and age distributions observed in plutons (Samperton et al., 2015). This predicts a peak in zircon crystallisation at the onset of zircon saturation which decays until the solidus, producing a skew towards older ages. However, this prediction assumes monotonous cooling of magma, while open-system behaviour can produce multi-modal age distributions with a general shift towards younger skew (Caricchi et al., 2014; Schmitt et al., 2023; Tavazzani et al., 2023a).

We use the approach of Tavazzani et al. (2023b) who generated zircon age distributions representative of complex crystallisation simulations. These simulations investigate zircon crystallisation under a range of non-linear temperature-crystallinity scenarios developed using the thermodynamic modelling software Magma Chamber Simulation (Bohrson et al., 2014). This combines closed- and open-system processes such as fractional crystallisation, single or repeated recharges of new magma in a magma body. Synthetic age distributions generated under varying recharge can then be compared to natural data as described above. We compare the bootstrap sampling of a zircon age distribution generated with recharge of a cooling, upper crustal rhyolitic magma reservoir with 0, 3 and 5 recharges. Each recharge is triggered when crystallinity reaches 50 vol.% and comprises an addition of 50 g of rhyolitic magma (with an initial magma reservoir mass of 100 g) with the same composition and liquidus temperature (870°C) as the original magma (Tavazzani et al., 2023b).

3   Results

The PCA plot of the W_2 dissimilarity matrix of the high precision U-Pb data compilation produces a parabolic shape (Figure 5). Because the W_2 distance is equivalent to the squared difference between two weighted ECDFs, the location of an age distribution on the plot of the PCA of the W_2 dissimilarity matrix (Fig. 5) can be compared with the shapes of the weighted ECDFs of the age distributions (Fig. 3). The distance between two age distributions on the PCA plot refers to the degree of dissimilarity between them. For example, two strongly contrasting distributions (Fig. 3) such as from a New England plutonic sample (old skew) and a Yellowstone volcanic sample (young skew) plot on opposite sides of the PC parabola (Fig. 5). By contrast, relatively homogeneous weighted ECDFs in single magmatic systems cluster together on the PC parabola (e.g. Toba).

There is a pronounced tendency for volcanic and porphyry zircon age distributions to plot further left on the parabola than plutonic age distributions which plot on the right (Fig. 5). In order to interpret this difference, we cast skewed normal distributions onto the W_2 dissimilarity matrix which were generated with varying values of skew (see inset plots in Fig. 5). This comparison demonstrates that the position of a distribution along the PC parabola generally reflects the amount of skew of a distribution, because old-skewed distributions plot in the top left of the parabola, whilst young-skewed distributions plot in the top right. Distributions that show a lack of skew (i.e. normal distributions) plot towards the centre of the parabola. Volcanic and porphyry age distributions therefore generally skew towards younger ages, whereas plutonic age distributions skew towards older ages.
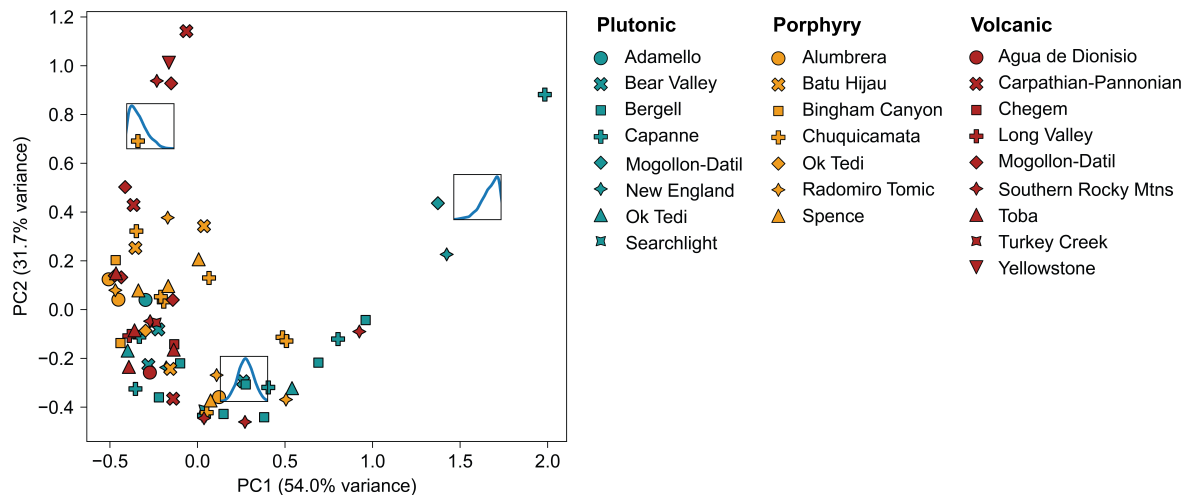
Figure 5. Results of PCA on the W_2 ID-TIMS zircon U-Pb dissimilarity matrix. Each data point indicates one U-Pb age distribution (i.e. one sample or unit) for a magmatic system. The percentage variance that each principal component accounts for is given. Three inset graphs represent KDEs of skew normal distribution with varying values of skew (-100, 0 and 100) for comparison with natural distributions.

4 Discussion

4.1 Controlling factors on zircon age distributions

260 #### 4.1.1 Analytical factors

As discussed previously, the ability to resolve geological dispersion from an age distribution depends strongly on $\Delta t/\sigma$. The apparent $\Delta t/\sigma$ threshold applied to our database (> 10) aims to reduce the number of age distributions which are dominated by analytical uncertainty. In order to validate our choice of apparent $\Delta t/\sigma$ filter, we examined the position of distributions on the PC parabola relative to their apparent $\Delta t/\sigma$ (Figure 6A). We do not find that low values of apparent $\Delta t/\sigma$ (i.e. close to 10) lead

265 to a collapse of distributions towards normal distributions, indicating that these distributions are unlikely to be dominated by analytical uncertainty. We additionally find that repeating our analysis with a lower threshold of apparent $\Delta t/\sigma$ (> 5) provides similar results (Fig. S4) yet further populates the central part of the parabola, potentially indicating these lower apparent $\Delta t/\sigma$ distributions have less skew and are thus dominated by analytical uncertainty.

We limited our study to young ID-TIMS datasets (< 130 Ma) where chemical abrasion was performed to reduce the affects of

270 Pb loss. However, we find that the conditions under which chemical abrasion was performed vary. Notably, the temperatures of chemical abrasion range between 180 and 220°C which can impact the measured U-Pb date (Widmann et al., 2019; McKanna et al., 2024). To exclude the possibility that the variability in shape of an age distribution could be the result of unmitigated Pb loss, we compiled the chemical abrasion temperature of zircon in each study, and compared this with the position of each distribution on the PCA plot of the W_2 dissimilarity matrix (Fig. S5). If unmitigated Pb loss is present, we should find that
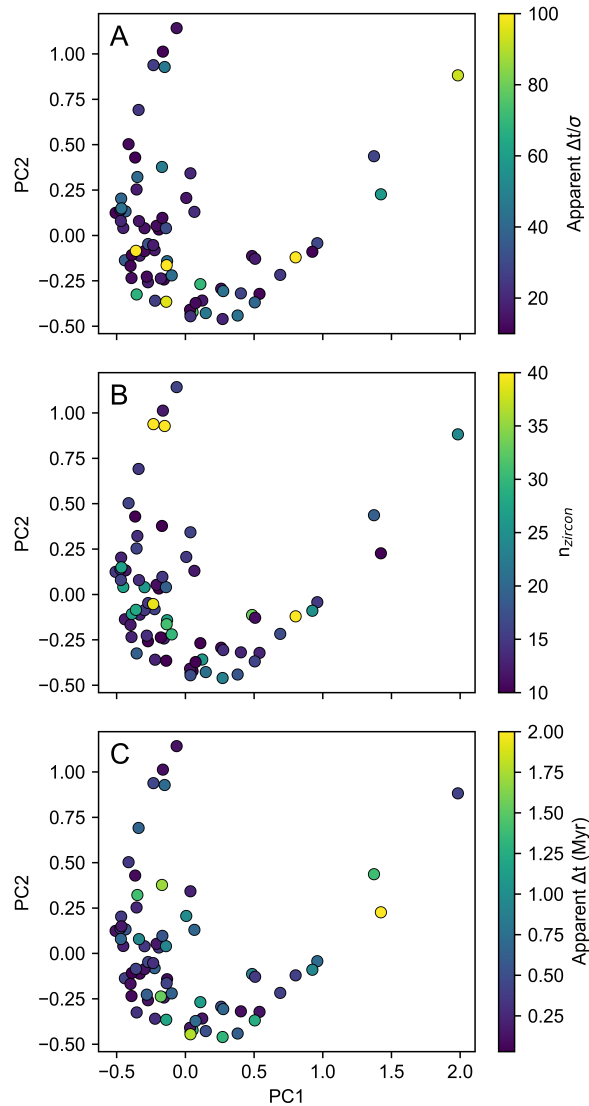
Figure 6. Plot of the PCA on the W_2 ID-TIMS zircon U-Pb dissimilarity matrix coloured by: (A) the ratio of zircon crystallisation duration and the mean analytical uncertainty (apparent $\Delta t/\sigma$), (B) the number of zircons in the age spectrum (n_{zircon}) and (C) the duration of zircon crystallisation in Myr (apparent Δt).

275 age distributions from lower chemical abrasion temperatures plot in the top right of the PC parabola. However, we find no relationship between chemical abrasion temperature and distribution shape, which negates the possibility that the varying shape of age distributions in CA-ID-TIMS datasets is related to unmitigated Pb loss.
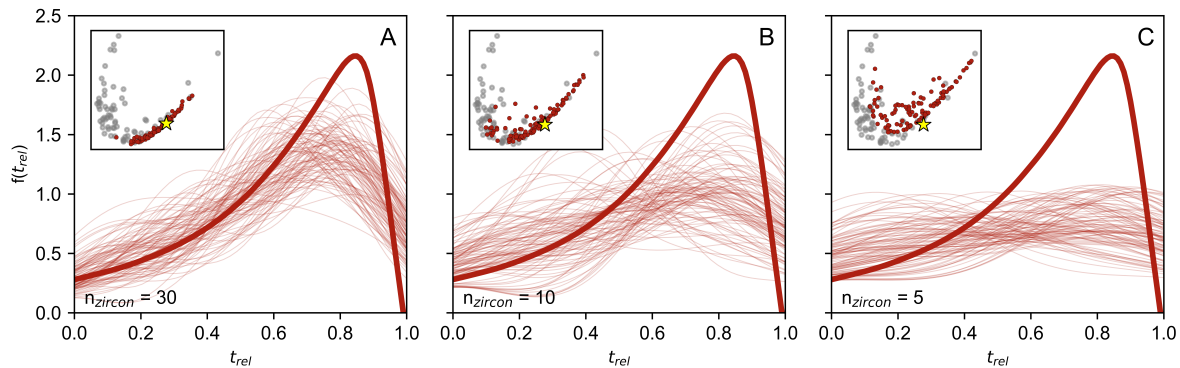
Figure 7. Kernel density plots showing results of bootstrap sampling of the theoretical zircon crystallisation distribution in a monotonically cooling magma reservoir derived from thermodynamic models (Keller et al., 2018) as shown by the thick red curve. The number of zircons sampled (n_{zircon}) ranges from (A) 30, (B) 10, to (C) 5 and the thin translucent red curves show 100 sampling iterations. An uncertainty is added to each age as appropriate for a sample at 10 Ma. Inset plots show the PCA of the W_2 dissimilarity matrix of natural zircon U-Pb distributions (grey symbols) and where the 100 synthetic age distributions plot (red symbols) relative to the sampled distribution (star).

4.1.2 Number of zircons sampled

A decreasing number of zircon analyses (n_{zircon}) in an age distribution leads to a collapse of an age distribution towards a nor-
280 mal distribution (Tavazzani et al., 2023a). To further test the validity of our choice of $n_{zircon} > 10$ as a filter, we systematically
study the effect of n_{zircon} by sampling different numbers of zircon from the same underlying synthetic zircon crystallization
distribution in a monotonically cooling magma reservoir derived from thermodynamic models (for a full description of the
methodology used to obtain this theoretical distribution see Keller et al. (2018); Tavazzani et al. (2023b)). We perform this
sampling for n_{zircon} of 5, 10 and 30 at analytical uncertainties typical for 10 Ma old zircons (Fig. 7) and provide a more ex-
285 tensive analysis at different zircon crystallization ages (Fig. S6) and for n_{zircon} between 4 and 60 (Fig. S7). Our search space
for n_{zircon} broadly reflects the lower, intermediate and upper range of zircon analysed per sample in the compiled ID-TIMS
datasets (Table S1).

Results of iterative sampling from an underlying monotonic cooling distribution highlight the loss of reproducibility of the
initial distribution when n_{zircon} = 5 (Fig. 7). This is reflected by the increasing flattening of the KDE curve and, in PCA space
290 of the W_2 dissimilarity matrix, by a scatter of synthetic zircon distributions towards highly variable positions on the PCA plot.
Undersampling of the underlying distribution can lead to a reversal of the skew in the bootstrapped distribution (i.e. plotting
on the left hand side of the PC parabola; Fig. 7). This confirms that the shape of age distributions in datasets where $n_{zircon} <$
10 should not be interpreted in the context of geological variability.

Sampling a larger number of zircons (n_{zircon} = 10) more accurately captures the skew towards older ages of the underlying
295 distribution (Fig. 7). However, an appreciable variation is still apparent in these sampled distributions which cover a large
range of PC1 scores in the W_2 dissimilarity matrix. With an even larger number of sampled zircon dates (n_{zircon} = 30), the

variance of the sampled distributions reduces as they more accurately reproduce the underlying distribution. However, even in the case where the number of sampled zircon dates is high (n = 30), significant variation still exists in the PCA plot of the W_2 dissimilarity matrix (Fig. 7). This finding suggests one should avoid making interpretations from small variations between different spectra on the PC parabola, since these are likely to reflect undersampling-related scatter.

More detailed modelling of the effect of n_{zircon} on the ability to capture an underlying age distribution (Fig. S7) shows that for 10 Ma old zircons, the optimal choice of n_{zircon} is approximately 14 because increasing n_{zircon} beyond this leads to only a marginal increase in performance. At 100 Ma, producing an equivalent performance requires approximately 20 zircon grains to be dated. However, our choice of n_{zircon} = 10 for this study can still capture an underlying distribution and a greater threshold would significantly impact the availability of natural data for this study. As larger datasets are published, the filtering threshold of n_{zircon} could be increased to further reduce the effect of undersampling on the shape of the age distribution.

4.1.3 Truncation of zircon crystallisation

Zircon age distributions in volcanic and porphyry rocks are produced by a characteristic crystallisation history, because magma quenching upon evacuation/eruption after zircon saturation will interrupt zircon crystallisation (Keller et al., 2018; Schmitt et al., 2023). We model the effect that 'truncation' has on the resulting zircon age spectra by using the same underlying monotonic cooling zircon crystallisation distribution used above, sampled at variable degrees of t_{rel}, namely 0.8, 0.5 and 0.1. This simulates scenarios where a monotonically cooling igneous body erupts at a time close to the solidus relative to zircon saturation (t_{rel} = 0.8), halfway in time between zircon saturation and the solidus (t_{rel} = 0.5) or close in time to the onset of zircon saturation (t_{rel} = 0.1). We model this range as volcanic products can vary between crystal-poor and crystal-rich (Hildreth, 1981) and porphyry rocks are typically crystal-rich, though we emphasise that t_{start} refers to the time of zircon saturation and not the liquidus. The simplified model assumes that melt quenches upon evacuation, thus abruptly terminating zircon crystallisation.

The zircon age distribution of a magma extracted at t_{rel} = 0.8 are comparable with the distribution obtained from a monotonically cooled magma body, although some of the skew toward older ages is lost (Fig. 8). These sampled synthetic distributions produced by mild truncation of the underlying monotonic cooling distribution reproduce the spread of the natural dataset on the right arm of the PC parabola. When truncation takes place at an intermediate time between zircon saturation and the system's solidus (t_{rel} = 0.5), the effect of truncation of the underlying monotonic cooling distribution is more evident. In this scenario, synthetic zircon age spectra lose most of their skew and largely overlap with the central axis of the natural zircon U-Pb distributions in the PC parabola (i.e. form a near-normal distribution). In the case of truncation happening at t_{rel} = 0.1, synthetic age distributions always exhibit young skew (i.e. plot on the left of the PC parabola). In the PCA space of the W_2 dissimilarity matrix, these simulation outputs do not overlap at all with the underlying monotonic cooling zircon age distribution.

These results indicate that truncation can significantly alter the shape of the underlying distribution, with extreme truncation (t_{rel} = 0.1 in our simplified model) being able to reverse the skew of a distribution. Our modelling also shows that truncation can account for most of the variability in zircon age distributions observed in natural examples. Therefore, this likely is a key factor in explaining the younger skew of volcanic and porphyry zircon age distributions relative to plutonic zircons, given the
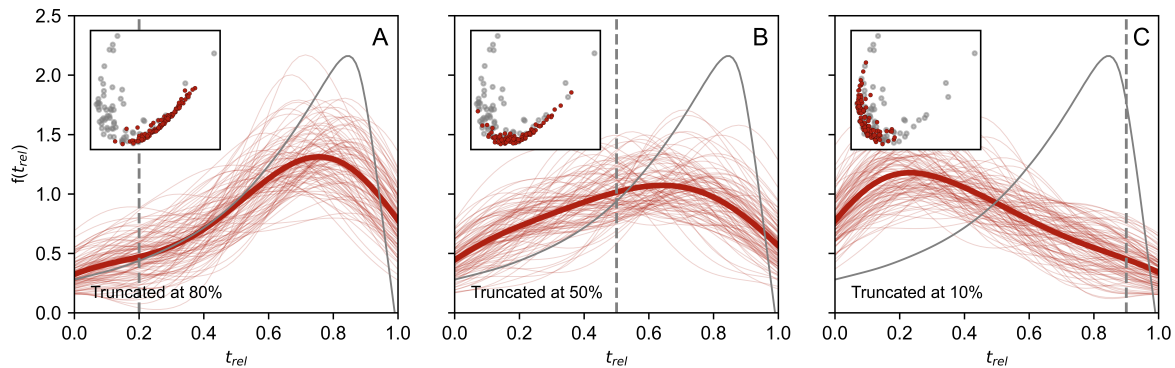
Figure 8. Modelled kernel density plots showing the effect of bootstrap sampling an underlying distribution with different degrees of truncation of zircon crystallisation (t_{rel} = 0.8; 0.5; 0.1) simulating melt extraction/volcanic eruption. The sampled underlying distribution (grey dashed line) is the monotonic cooling distribution (Keller et al., 2018). Thirty zircons are sampled for each of the 100 synthetic distribution (faint red) and the average of 100 simulations is shown (dark red). Inset plots show the location of these distributions (red symbols) in the PCA plot of the W_2 dissimilarity matrix of natural zircon U-Pb distributions (grey symbols).

former age distributions will be interrupted by magma evacuation and subsequent rapid cooling. We note however that even the most extreme effects of truncation are not able to reproduce a minority of volcanic zircon age spectra nested on the far top-left end of the PC parabola (Fig. 8).

4.1.4 Magma recharge

335 It has been suggested previously that differences in zircon age distributions between volcanic and plutonic systems may be linked to different fluxes in the source magma reservoir (Caricchi et al., 2014; Schmitt et al., 2023). The forward crystallization models investigated so far assume a monotonically cooling magma reservoir without subsequent recharge (Figs. 7 and 8), which may be unrealistic for many magmatic systems (Sparks et al., 1977), where recharge will increase temperature, change melt composition, and thus influence zircon crystallisation in the magmatic system (Szymanowski et al., 2020; Tavazzani

340 et al., 2023a). We therefore consider the role of sampling different underlying distributions of zircon ages whose shape may be produced by different magma recharge histories. In these scenarios, the compositional and thermal contribution of each new magma injection acts against zircon saturation and consequently delays zircon crystallisation.

We investigate the effects of an increasing number of rhyolitic melt recharges (0, 3 and 5 recharges of 870 °C) into a cooling rhyolitic magma reservoir. The underlying distributions transition from unimodal with no recharge, to increasingly multi-modal

345 and with younger skew as the number of recharges increases (Fig. 9). With no recharge, the synthetic zircon crystallisation spectrum is equivalent to the monotonic cooling distribution and sampled distributions all exhibit older skew and are located on the right hand side of the PC parabola. With three recharges, the synthetic distributions have predominantly younger skew and plot towards the centre and left of the PC parabola (Fig. 9). With five recharges, the synthetic distributions look broadly
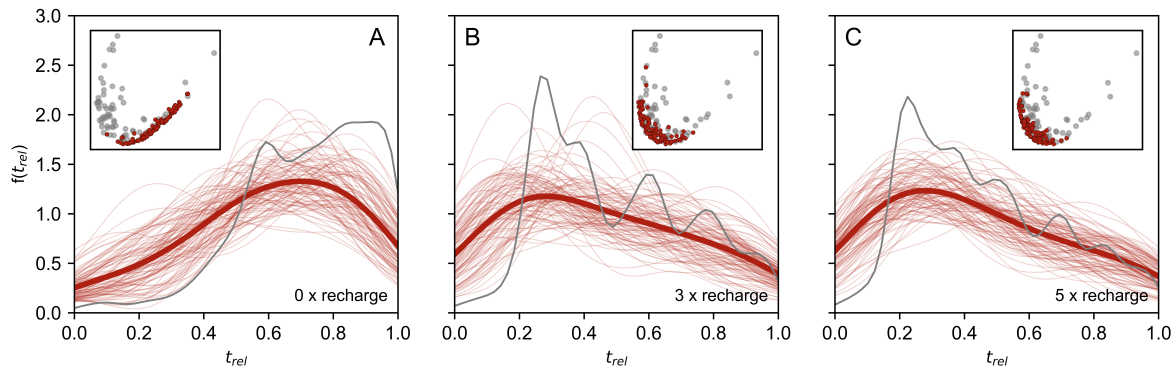
Figure 9. Modelled kernel density curves showing the effect of repeated magma recharge on zircon age distributions. Underlying zircon age distributions produced with varying numbers of recharges of felsic melt into a felsic magma reservoir undergoing cooling and crystallisation. Underlying zircon age distributions (grey curves) are taken from Tavazzani et al. (2023b) for (A) 0, (B) 3, and (C) 5 recharge events during magma cooling. Thirty zircons are sampled from each on of the 100 sampled distributions and uncertainties are added as appropriate for 10 Ma old zircons (red curves). The average curve (thick opaque red) shows the average of the 100 synthetic age distributions and the progressive shift from old to young skew with increasing number of recharges. Insets show the location of these distributions (red symbols) in the PCA plot of the W_2 dissimilarity matrix of natural zircon U-Pb distributions (grey symbols).

similar to those after three recharges, but with less variance and a slight increase in the skew towards younger ages (Fig. 9). Therefore, magma recharge appears to exert a strong control on the skew of zircon age distributions, in a similar albeit less extreme manner to truncation of zircon crystallisation. Furthermore, like truncation, it is unable to produce the age distributions plotting at the extreme top left of the PC parabola.

4.1.5   Incorporation of antecrystal zircon

The natural age distributions that plot at the extreme top left of the PC parabola (Fig. 5) are those with a minority of zircon dates that are significantly older than the main population. Because these age distributions can't be reproduced by the modelling performed so far, it is possible these distributions contain "antecrysts" (Miller et al., 2007) that are only marginally older than the broader age distribution (and hence not identified by our filtering method). An inspection of the ECDFs of these age distributions (Fig. 3) indicates that they contain a small number of zircons (1–3) that could be from an older population.

The modelling presented so far samples an age distribution from a single magma reservoir. To model the effect of "antecrysts" on zircon age distributions, we additionally sample n_{inh} zircons from a second age distribution which is older than the primary age distribution in relative time by Δt_{rel}. The population of n_{inh} is then added to a primary bootstrapped age distribution consisting of $n_{zircon} - n_{inh}$ zircons and then t_{rel} is renormalised between zero and one. These modelled age distributions can then be treated identically to those modelled above, and compared with natural data in the PCA W_2 space.
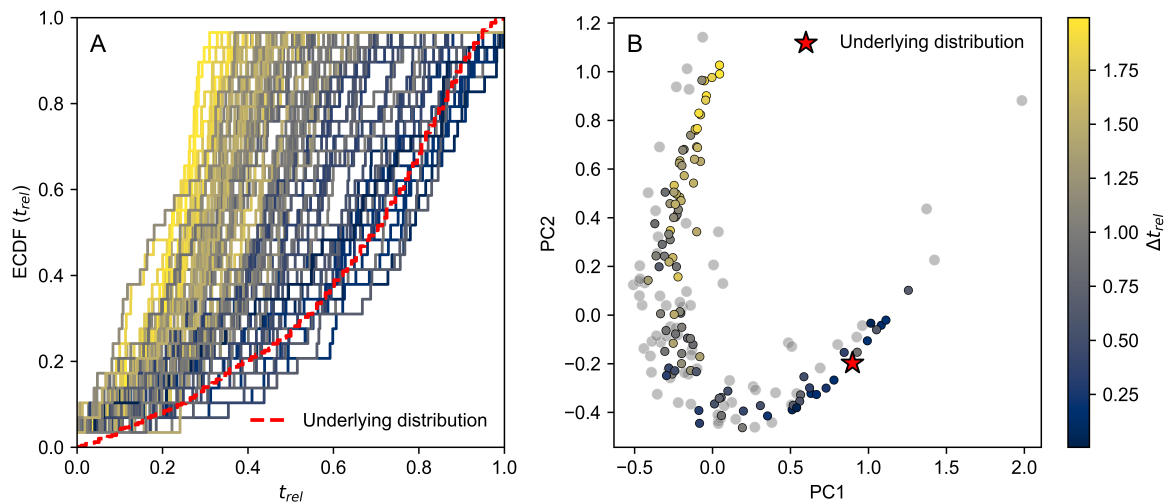
Figure 10. The effect of antecrysts on zircon age distributions for 100 simulations where 29 zircons are sampled from a primary age distribution and one zircon is sampled from an identical age distribution older by Δt_{rel} from the primary distribution. Δt_{rel} is randomly varied between 0 and 2 and each synthetic distribution is coloured by the magnitude of Δt_{rel}. (A) The ECDF of each synthetic distribution and (B) the location of each synthetic distribution in the PCA plot of the W_2 dissimilarity matrix of natural zircon U–Pb distributions. A large number of these synthetic distributions would be filtered for the antecryst when the outlier filtering method in Section 2.2 is employed (Fig. S8).

Our modelling of the effect of sampling antecrysts on age distributions shows that the presence of just one antecrystic zircon
365 in an autocrystic population of 30 zircon U-Pb dates can have a profound effect on the final age distribution (Fig. 10). An antecryst derived from an older secondary age distribution where $\Delta t_{rel} = 1$ (i.e. zircon crystallisation in older distribution ended at the same time as zircon saturation in the primary, younger distribution) has a discernible effect on the age distribution, shifting it from plotting alongside older skewed datasets to where those with normal distributions plot (Fig. 10). Larger values of Δt_{rel} (up to two) have an even greater effect, and can produce the extreme top left end of the PC parabola produced by the
370 natural data.

In summary, our modelling suggests that truncation of zircon crystallisation is the most likely candidate to explain the difference between volcanic, porphyry and plutonic zircon age distributions because it is a factor that affects all volcanic and porphyry zircon age distributions and does not affect plutonic distributions. Variable magma recharge will also play a significant role yet is not required to explain the variability in natural age distributions. The most extreme young skewed age distributions
375 can be attributed to the incorporation of "antecrysts" in an age distribution. In reality, the observed zircon age spectra can be simultaneously affected by many of the geological and analytical effects discussed here, and the deconvolution of their exact contributions will be challenging.

4.2 Implications for the estimation of eruption/solidification ages

The most common application of zircon age spectra is to calculate t_{end}, i.e. the age of a volcanic eruption or emplacement of an intrusion (Keller et al., 2018; Ratschbacher et al., 2018). Although many authors often use the youngest measured date or the weighted mean of the youngest population of dates, Keller et al. (2018) demonstrated that a Bayesian method frequently provides the most accurate result and is least likely to underestimate uncertainty on the eruption or emplacement age.

The Bayesian approach uses prior knowledge of the zircon crystallisation spectrum (e.g. from theoretical constraints), measured zircon U-Pb age data and their uncertainties to estimate t_{end} and its uncertainty. Several options exist for prior distributions such as the monotonic cooling distribution, a uniform distribution or a bootstrapped sample of the measured U-Pb dates. In some cases, the choice of prior may not greatly influence the eruption age (Keller et al., 2018), but in cases where the data are under-dispersed, analytical uncertainties are high, or the number of zircons is low, greater importance is placed on a prior knowledge of the zircon age distribution. Therefore, our analysis of natural zircon age distributions from young systems can inform the choice of a prior distribution. Our study shows that a monotonic cooling distribution (skew towards old ages) can be assumed for many plutonic systems but is not appropriate for volcanic or porphyry systems (Fig. 5). For volcanic and porphyry systems, a truncated distribution appears to be the most appropriate choice of prior (e.g. truncated normal, half normal or triangular distributions; Keller (2018)) as validated by our modelling of the effect of truncation on shifting zircon age spectra towards a younger skew (Fig. 8).

4.3 Resolving zircon age distributions using different analytical techniques

The effect of geological processes versus analytical uncertainty on an age distribution will vary as a function of sample age (i.e. as absolute analytical uncertainties expand). The interpretations made in this study are based on relatively young (*ca.* < 130 Ma) magmatic systems analysed by ID-TIMS, where analytical capabilities are strongest and the potential for Pb loss is lowest. However, it is also possible that such an approach could be applicable to *in situ* techniques such as LA-ICP-MS for samples young enough that the large relative analytical uncertainties inherent to the technique correspond to sufficiently low absolute uncertainties.

We adapt our bootstrap model of the monotonic cooling age distribution to sample age distributions at a wider range of ages (between 0.1 and 1000 Ma) for absolute analytical uncertainties relevant to ID-TIMS and LA-ICP-MS at the given age. This uses the parametrisation of ID-TIMS uncertainties as a function of age (Equation 8) to allow the bootstrap modelling of the monotonic cooling distribution to be performed from 0.1 to 1000 Ma. We also performed a third-order polynomial regression on 2σ absolute uncertainties reported for a compilation (Chelle-Michou and Schaltegger, 2023) of LA-ICP-MS dates (*t* in Ma) up to 1000 Ma with uncertainties reported as 2*SE*:

$$2\sigma = 4.0 \times 10^{-8}(\pm 8.6 \times 10^{-9})t^3 - 4.1 \times 10^{-5}(\pm 1.0 \times 10^{-5})t^2 + 0.024(\pm 0.0029)t + 0.22(\pm 0.14) \qquad (9)$$

Gaussian uncertainty is propagated onto each date sampled during bootstrap sampling according to the standard error on the fit parameters. We perform bootstrap sampling 25 times and calculate the Wasserstein distance between the sampled age
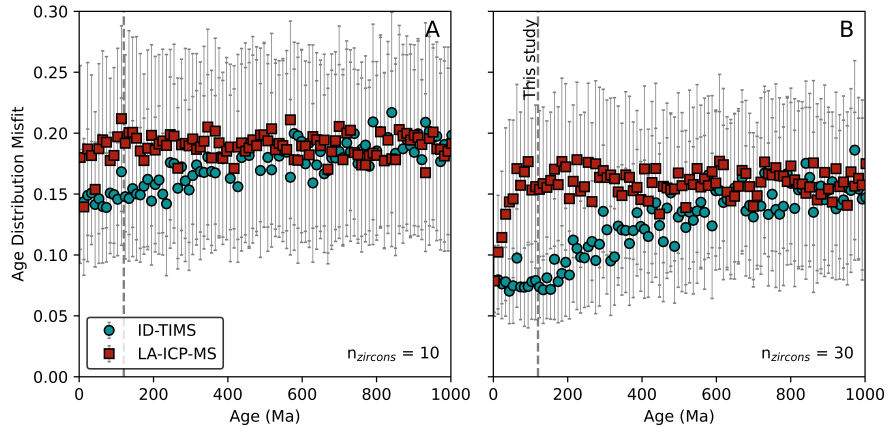
Figure 11. Comparison of the ability of ID-TIMS and LA-ICP-MS to capture the underlying zircon age distribution. At a given age, bootstrap forward modelling is applied on the monotonic cooling age distribution (Keller et al., 2018) and the Wasserstein distance is calculated between the sampled age distribution and the underlying distribution. At each age this is repeated 25 times and the mean W_2 is shown with the error bars showing the standard deviation. Vertical dashed line shows the maximum age of ID-TIMS distributions permitted in this study. This method is repeated for A) $n_{zircon} = 10$ and B) $n_{zircon} = 30$.

410 distribution and the original age distribution which we refer to as the age distribution "misfit" (Figs. 11, and S9). We average and plot these 25 misfit scores along with their standard deviation. When the misfit is 0, the bootstrap sampled age distribution fully reproduces the underlying distribution. As the bootstrapped distribution deviates further from the underlying distribution, the misfit increases.

  When 10 zircon crystals are sampled, this analysis indicates that at young ages (<5 Ma), LA-ICP-MS and ID-TIMS can cap-
415 ture the underlying distribution to a similar degree. When 30 zircon crystals are sampled, the overlap of analytical performance between LA-ICP-MS and ID-TIMS is only present at very young ages (<1 Ma). This indicates that for the youngest systems, it may be possible to resolve a zircon age distribution using LA-ICP-MS where high n_{zircon} datasets can be more easily ac-quired, though we emphasise this requires further study since reported LA-ICP-MS uncertainties may be underestimated and often do not fully account for 'matrix effects' (e.g. laser- and plasma-induced fractionation, reflected in 1-2 % long-term excess
420 uncertainties) (Large et al., 2020; Sliwinski et al., 2022). With increasing age, the absolute precision of LA-ICP-MS decreases linearly, as evidenced by the rapid increase in misfit between 0 and *ca* 100 Ma for $n_{zircon} = 10$. For ages older than this, the misfit remains unchanged with increasing age because analytical uncertainties dominate the sampled distribution, forming a normal distribution. By contrast, for ID-TIMS, the misfit increases less rapidly with age. This continues until approximately 500 Ma, when the misfit is equivalent to LA-ICP-MS and the sampled dates form a normal distribution regardless of the shape
425 of the underlying distribution.

4.4 Comparisons with thermal modelling of zircon age distributions

Zircon U-Pb age distributions provide the most robust time-resolved history of magmatic systems. Several studies have used these spectra in combination with thermal models to understand the dynamics of magma reservoirs, such as by quantifying the magmatic flux and the duration of magmatism (Caricchi et al., 2014; Tierney et al., 2016; Weber et al., 2020; Schmitt et al., 2023). Though initially such models assumed linear zircon crystallisation after zircon saturation (Caricchi et al., 2014, 2016), some recent models have taken into account the thermal and compositional dependence of zirconium solubility in a silicic melt and its effect on zircon saturation (Tierney et al., 2016; Schmitt et al., 2023). The generally older skew of plutonic age distributions observed in our analyses is consistent with that predicted from zircon solubility and thermodynamic models on a monotonically cooling magma reservoir (Watson, 1996; Keller et al., 2018, Fig. 7). However, thermal models that take into account incremental pluton assembly and heat transfer produce age distributions on a reservoir scale with young skew (e.g. Schmitt et al., 2023) which is at odds with our observation from natural plutonic rocks.

The discrepancy between natural plutonic age distributions (old skew) and thermal modelling of zircon age distributions (young skew) may be the result of several factors. Thermal modelling papers consider zircon age distributions at the reservoir scale, where slow cooling and heat transfer may delay the overall peak zircon crystallisation towards the solidus (young skew). However, the incremental assembly of such plutons may mean that on a localised scale relevant to that from which a hand sample may originate, the melt may cool rapidly and according to monotonic cooling and lead to older skew of zircon age distributions in a single sample. We note however that the >100 kyr durations of zircon crystallisation recorded by plutons may not be achieved by cooling of small melt batches, which could rather be explained by the bulk of zircon crystallising deeper than the emplacement level (Barboni et al., 2015; Nathwani et al., 2024). An additional bias is that a small number of datasets (Barboni et al., 2015; Samperton et al., 2015) contain sub-grain analyses which can skew the age distribution to older ages (Klein and Eddy, 2023), such as in the case of (Samperton et al., 2015) where cores show considerably older ages than rims (up to 500 kyr). However, old skew is observed in plutonic age distributions where cores were not analysed in isolation (e.g., Barboni et al., 2015; Kinney et al., 2021) suggesting it may not be a primary factor. Lastly, melt extraction from magma mush in the plutonic environment (e.g. to eruptions/dykes) may remove the youngest-crystallised zircon, leading to a dominance of early-crystallised zircon in the remaining intrusion. By contrast, zircons in volcanic rocks may represent the mixing of zircons crystallised throughout the entire magma reservoir, producing an age distribution more dominated by heat transfer (i.e. a younger skew).

Previous studies based on a more limited dataset have also noticed the young-skewed zircon age distributions in volcanic systems relative to plutonic systems (Caricchi et al., 2014; Tavazzani et al., 2023a). This has been used to suggest volcanic systems have non-linear thermal histories and overall higher magma recharge rates (Caricchi et al., 2014; Tierney et al., 2016; Schmitt et al., 2023; Tavazzani et al., 2023a). However, our study indicates that these young skewed zircon age spectra can also be produced by the truncation of zircon crystallisation by a volcanic eruption. Thus, we emphasise that decoupling the effects of recharge and truncation is challenging, and magmatic fluxes inverted from volcanic age distributions should be treated with caution, particularly when contrasted with plutonic age distributions. However, between plutonic systems (where truncation is

460 not a large factor) it may be possible to more robustly quantify magma recharge rates using zircon age spectra. Future work on retrieving information on magma dynamics from zircon age spectra may therefore be best suited to younger plutonic systems (e.g. Barboni et al., 2015; Farina et al., 2024).

5 Conclusions

We provide a quantitative framework to compare high-precision zircon U-Pb age distributions of igneous samples using the
465 Wasserstein distance, and show that this statistical measure accurately captures differences in shape between age distributions. Our study provides a comprehensive analysis of a large database of CA-ID-TIMS data from 22 different magmatic systems. We filter our data compilation to isolate datasets where relative uncertainties permit resolution of geological dispersion. The filtering approach includes a new method to systematically filter the tails of age distributions in large datasets. Exploring the effect of geological processes on age distributions is made challenging by varying ratios of zircon crystallisation duration to
470 analytical precision ($\Delta t/\sigma$) and varying numbers of sampled zircons. Notwithstanding these limitations, our analysis of natural data indicates clear geological differences between volcanic, porphyry and plutonic age distributions where volcanic and porphyry zircon age distributions exhibit younger skew and plutonic exhibit older skew. We adopt a bootstrap modelling approach which generates synthetic distributions and permits comparison with natural distributions according to the Wasserstein distance. This analysis indicates that the younger skew of volcanic and porphyry age distributions can be best explained by
475 variable degree of truncation of zircon crystallisation by a volcanic eruption or porphyry dyke emplacement. We also show that magma recharge can contribute towards the younger skew of volcanic and porphyry age distributions, though we suggest that the role of truncation is most important. This major control of zircon crystallisation truncation on an age distribution suggests that interpreting magma dynamics (e.g. quantifying magmatic fluxes) from volcanic age distributions may be challenging, and such an approach is more appropriate for plutonic age distributions. As analytical precision improves and increasing num-
480 bers and sizes of CA-ID-TIMS zircon U-Pb datasets are published, our framework will facilitate improved interpretation of geological information from zircon age distributions.

Code and data availability. The code to reproduce the findings of this study is deposited in open-source Zenodo repository (https://doi.org/10.5281/zenodo.13378412). The database of zircon age distributions is provided in the Supplementary Data (Table S1) and deposited in the Zenodo repository.

485 *Author contributions.* Conceptualisation: CN, DS, LT. Data curation: CN, DS, LT, SM, AV. Formal analysis: CN. Software: CN. Investigation: CN, DS, LT. Methodology: CN, LT, DS, CCM. Resources - CCM. Writing – original draft preparation: CN, DS, LT. Writing – review & editing: SM, AV, CCM.

Competing interests. The authors have no competing interests to declare

Acknowledgements. This study was funded by an ETH Zurich Postdoctoral Fellowship (22-1 FEL-21) and by Swiss National Science
490   Foundation grants 200021L_219300 and 200021_212892. CN thanks Alex Lipp for insightful discussions on the Wasserstein distance. Ryan
Ickert and an anonymous reviewer are thanked for their constructive reviews of this manuscript, and Brenhin Keller is thanked for editorial
handling. Informal reviews of this manuscript by Luca Caricchi, Zoe Moser and Alex Lipp are also gratefully acknowledged.

References

Barboni, M., Annen, C., and Schoene, B.: Evaluating the construction and evolution of upper crustal magma reservoirs with coupled U/Pb zircon geochronology and thermal modeling: A case study from the Mt. Capanne pluton (Elba, Italy), Earth and Planetary Science Letters, 432, 436–448, https://doi.org/10.1016/j.epsl.2015.09.043, 2015.

Bindeman, I. N., Wotzlaw, J. F., Stern, R. A., Chiaradia, M., Guillong, M., and Colón, D. P.: Geochronology and geochemistry data for the Elbrus, Tyrnyauz, and Chegem magmatic centers, Greater Caucasus, Russia, Data in Brief, 35, 106 896, https://doi.org/10.1016/j.dib.2021.106896, 2021.

Bohrson, W. A., Spera, F. J., Ghiorso, M. S., Brown, G. A., Creamer, J. B., and Mayfield, A.: Thermodynamic model for energy-constrained open-system evolution of crustal magma bodies undergoing simultaneous recharge, assimilation and crystallization: the Magma Chamber Simulator, Journal of Petrology, 55, 1685–1717, https://doi.org/10.1093/petrology/egu036, 2014.

Brlek, M., Richard Tapster, S., Schindlbeck-Belo, J., Gaynor, S. P., Kutterolf, S., Hauff, F., Georgiev, S. V., Trinajstić, N., Šuica, S., Brčić, V., Wang, K.-L., Lee, H.-Y., Beier, C., Abersteiner, A. B., Mišur, I., Peytcheva, I., Kukoč, D., Németh, B., Trajanova, M., Balen, D., Guillong, M., Szymanowski, D., and Lukács, R.: Tracing widespread Early Miocene ignimbrite eruptions and petrogenesis at the onset of the Carpathian-Pannonian Region silicic volcanism, Gondwana Research, 116, 40–60, https://doi.org/10.1016/j.gr.2022.12.015, 2023.

Brown, S. J. A. and Fletcher, I. R.: SHRIMP U-Pb dating of the preeruption growth history of zircons from the 340 ka Whakamaru Ignimbrite, New Zealand: Evidence for >250 k.y. magma residence times, Geology, 27, 1035, https://doi.org/10.1130/0091-7613(1999)027<1035:SUPDOT>2.3.CO;2, 1999.

Bunker, E.: The hypogene evolution of the Spence porphyry copper deposit, northern Chile, PhD thesis, University of Bristol, https://research-information.bris.ac.uk/en/studentTheses/the-hypogene-evolution-of-the-spence-porphyry-copper-deposit-nort, 2020.

Buret, Y., von Quadt, A., Heinrich, C., Selby, D., Wälle, M., and Peytcheva, I.: From a long-lived upper-crustal magma chamber to rapid porphyry copper emplacement: Reading the geochemistry of zircon crystals at Bajo de la Alumbrera (NW Argentina), Earth and Planetary Science Letters, 450, 120–131, https://doi.org/10.1016/j.epsl.2016.06.017, 2016.

Buret, Y., Wotzlaw, J.-F., Roozen, S., Guillong, M., von Quadt, A., and Heinrich, C. A.: Zircon petrochronological evidence for a plutonic-volcanic connection in porphyry copper deposits, Geology, 45, 623–626, https://doi.org/10.1130/G38994.1, 2017.

Caricchi, L., Simpson, G., and Schaltegger, U.: Zircons reveal magma fluxes in the Earth's crust, Nature, 511, 457–461, https://doi.org/10.1038/nature13532, 2014.

Caricchi, L., Simpson, G., and Schaltegger, U.: Estimates of volume and magma input in crustal magmatic systems from zircon geochronology: the effect of modeling assumptions and system variables, Frontiers in Earth Science, 4, https://doi.org/10.3389/feart.2016.00048, 2016.

Chelle-Michou, C. and Schaltegger, U.: U–Pb Dating of Mineral Deposits: From Age Constraints to Ore-Forming Processes, in: Isotopes in Economic Geology, Metallogenesis and Exploration, edited by Huston, D. and Gutzmer, J., pp. 37–87, Springer International Publishing, Cham, https://doi.org/10.1007/978-3-031-27897-6_3, 2023.

Curry, A., Gaynor, S. P., Davies, J. H. F. L., Ovtcharova, M., Simpson, G., and Caricchi, L.: Timescales and thermal evolution of large silicic magma reservoirs during an ignimbrite flare-up: perspectives from zircon, Contributions to Mineralogy and Petrology, 176, 103, https://doi.org/10.1007/s00410-021-01862-w, 2021.

Deering, C. D., Keller, B., Schoene, B., Bachmann, O., Beane, R., and Ovtcharova, M.: Zircon record of the plutonic-volcanic connection and protracted rhyolite melt evolution, Geology, 44, 267–270, https://doi.org/10.1130/G37539.1, 2016.

530   Eddy, M. P., Pamukçu, A., Schoene, B., Steiner-Leach, T., and Bell, E. A.: Constraints on the timescales and processes that led to high-SiO2 rhyolite production in the Searchlight pluton, Nevada, USA, Geosphere, 18, 1000–1019, https://doi.org/10.1130/GES02439.1, 2022.

Farina, F., Dini, A., Davies, J. H., Ovtcharova, M., Greber, N. D., Bouvier, A.-S., Baumgartner, L., Ulianov, A., and Schaltegger, U.: Zircon petrochronology reveals the timescale and mechanism of anatectic magma formation, Earth and Planetary Science Letters, 495, 213–223, https://doi.org/10.1016/j.epsl.2018.05.021, 2018.

535   Farina, F., Weber, G., Hartung, E., Rubatto, D., Forni, F., Luisier, C., and Caricchi, L.: Magma flux variations triggering shallow-level emplacement of the Takidani pluton (Japan): Insights into the volcanic-plutonic connection, Earth and Planetary Science Letters, 635, 118 688, https://doi.org/10.1016/j.epsl.2024.118688, 2024.

Flamary, R., Courty, N., Gramfort, A., Alaya, M. Z., Boisbunon, A., Chambon, S., Chapel, L., Corenflos, A., Fatras, K., Fournier, N., Gautheron, L., Gayraud, N. T. H., Janati, H., Rakotomamonjy, A., Redko, I., Rolet, A., Schutz, A., Seguy, V., Sutherland, D. J., Tavenard,

540   R., Tong, A., and Vayer, T.: POT: Python Optimal Transport, Journal of Machine Learning Research, 22, 1–8, http://jmlr.org/papers/v22/20-451.html, 2021.

Gagnevin, D., Daly, J. S., and Kronz, A.: Zircon texture and chemical composition as a guide to magmatic processes and mixing in a granitic environment and coeval volcanic system, Contributions to Mineralogy and Petrology, 159, 579–596, https://doi.org/10.1007/s00410-009-0443-0, 2010.

545   Gaynor, S. P., Smith, T. M., and Schaltegger, U.: Tracing magmatic genesis and evolution through single zircon crystals from successive supereruptions from the Socorro Caldera Complex, USA, Earth and Planetary Science Letters, 616, 118 236, https://doi.org/10.1016/j.epsl.2023.118236, 2023.

Hildreth, W.: Gradients in silicic magma chambers: Implications for lithospheric magmatism, Journal of Geophysical Research: Solid Earth, 86, 10 153–10 192, https://doi.org/10.1029/JB086iB11p10153, 1981.

550   Ickert, R. B., Mundil, R., Magee, C. W., and Mulcahy, S. R.: The U–Th–Pb systematics of zircon from the Bishop Tuff: A case study in challenges to high-precision Pb/U geochronology at the millennial scale, Geochimica et Cosmochimica Acta, 168, 88–110, https://doi.org/10.1016/j.gca.2015.07.018, 2015.

Irpino, A. and Romano, E.: Optimal histogram representation of large data sets: Fisher vs piecewise linear approximation, https://www.semanticscholar.org/paper/Optimal-histogram-representation-of-large-data-vs-Irpino-Romano/8d599e43066c27a7128ea36db83b434816d39281, 2007.

555   Keller, C., Schoene, B., and Samperton, K.: A stochastic sampling approach to zircon eruption age interpretation, Geochemical Perspectives Letters, pp. 31–35, https://doi.org/10.7185/geochemlet.1826, 2018.

Keller, C. B.: Chron.jl: A Bayesian framework for integrated eruption age and age-depth modelling, https://doi.org/10.17605/OSF.IO/TQX3F, 2018.

560   Kinney, S. T., MacLennan, S. A., Keller, C. B., Schoene, B., Setera, J. B., VanTongeren, J. A., and Olsen, P. E.: Zircon U-Pb Geochronology Constrains Continental Expression of Great Meteor Hotspot Magmatism, Geophysical Research Letters, 48, e2020GL091 390, https://doi.org/10.1029/2020GL091390, 2021.

Klein, B. Z. and Eddy, M. P.: What's in an age? Calculation and interpretation of ages and durations from U-Pb zircon geochronology of igneous rocks, Geological Society of America Bulletin, https://doi.org/10.1130/B36686.1, 2023.

565   Large, S. J. E., von Quadt, A., Wotzlaw, J.-F., Guillong, M., and Heinrich, C. A.: Magma evolution leading to porphyry Au-Cu mineralization at the Ok Tedi deposit, Papua New Guinea: Trace element geochemistry and high-precision geochronology of igneous zircon, Economic Geology, 113, 39–61, https://doi.org/10.5382/econgeo.2018.4543, 2018.

Large, S. J. E., Wotzlaw, J.-F., Guillong, M., von Quadt, A., and Heinrich, C. A.: Resolving the timescales of magmatic and hydrothermal processes associated with porphyry deposit formation using zircon U–Pb petrochronology, Geochronology, 2, 209–230, https://doi.org/10.5194/gchron-2-209-2020, 2020.

Large, S. J. E., Buret, Y., Wotzlaw, J. F., Karakas, O., Guillong, M., von Quadt, A., and Heinrich, C. A.: Copper-mineralised porphyries sample the evolution of a large-volume silicic magma reservoir from rapid assembly to solidification, Earth and Planetary Science Letters, 563, 116 877, https://doi.org/10.1016/j.epsl.2021.116877, 2021.

Lipp, A. and Vermeesch, P.: Short communication: The Wasserstein distance as a dissimilarity metric for comparing detrital age spectra and other geological distributions, Geochronology, 5, 263–270, https://doi.org/10.5194/gchron-5-263-2023, 2023.

Liu, P.-P., Caricchi, L., Chung, S.-L., Li, X.-H., Li, Q.-L., Zhou, M.-F., Lai, Y.-M., Ghani, A. A., Sihotang, T., Sheldrake, T. E., and Simpson, G.: Growth and thermal maturation of the Toba magma reservoir, Proceedings of the National Academy of Sciences, 118, e2101695 118, https://doi.org/10.1073/pnas.2101695118, publisher: Proceedings of the National Academy of Sciences, 2021.

Markovic, S., Wotzlaw, J.-F., Szymanowski, D., Reuteler, J., Zeng, P., and Chelle-Michou, C.: μID-TIMS: Spatially-resolved high-precision U-Pb zircon geochronology, Geochronology Discussions, pp. 1–30, https://doi.org/10.5194/gchron-2024-17, publisher: Copernicus GmbH, 2024.

McKanna, A. J., Schoene, B., and Szymanowski, D.: Geochronological and geochemical effects of zircon chemical abrasion: insights from single-crystal stepwise dissolution experiments, Geochronology, 6, 1–20, 2024.

McLean, N. M., Bowring, J. F., and Bowring, S. A.: An algorithm for U-Pb isotope dilution data reduction and uncertainty propagation, Geochemistry, Geophysics, Geosystems, 12, Q0AA18, https://doi.org/10.1029/2010GC003478, 2011.

Miller, J. S., Matzel, J. E., Miller, C. F., Burgess, S. D., and Miller, R. B.: Zircon growth and recycling during the assembly of large, composite arc plutons, Journal of Volcanology and Geothermal Research, 167, 282–299, https://doi.org/10.1016/j.jvolgeores.2007.04.019, 2007.

Monge, G.: Memoire sur la theorie des deblais et des remblais, Mem. Math. Phys. Acad. Royale Sci., pp. 666–704, https://cir.nii.ac.jp/crid/1572261550791499008, 1781.

Nathwani, C., Blundy, J., Large, S. J. E., Wilkinson, J. J., Buret, Y., Loader, M. A., Tavazzani, L., and Chelle-Michou, C.: A zircon case for super-wet arc magmas, Nature Communications, 15, 8982, https://doi.org/10.1038/s41467-024-52786-5, publisher: Nature Publishing Group, 2024.

Pamukçu, A. S., Schoene, B., Deering, C. D., Keller, C. B., and Eddy, M. P.: Volcano-pluton connections at the Lake City magmatic center (Colorado, USA), Geosphere, 18, 1435–1452, https://doi.org/10.1130/GES02467.1, 2022.

Pedregosa, F., Varoquaux, G., Gramfort, A., Michel, V., Thirion, B., Grisel, O., Blondel, M., Prettenhofer, P., Weiss, R., Dubourg, V., Vanderplas, J., Passos, A., Cournapeau, D., Brucher, M., Perrot, M., and Duchesnay, : Scikit-learn: Machine Learning in Python, Journal of Machine Learning Research, 12, 2825–2830, http://jmlr.org/papers/v12/pedregosa11a.html, 2011.

Ratschbacher, B. C., Keller, C. B., Schoene, B., Paterson, S. R., Anderson, J. L., Okaya, D., Putirka, K., and Lippoldt, R.: A new workflow to assess emplacement duration and melt residence time of compositionally diverse magmas emplaced in a sub-volcanic reservoir, Journal of Petrology, https://doi.org/10.1093/petrology/egy079, 2018.

Rioux, M., Farmer, G. L., Bowring, S. A., Wooton, K. M., Amato, J. M., Coleman, D. S., and Verplanck, P. L.: The link between volcanism and plutonism in epizonal magma systems; high-precision U–Pb zircon geochronology from the Organ Mountains caldera and batholith, New Mexico, Contributions to Mineralogy and Petrology, 171, 13, https://doi.org/10.1007/s00410-015-1208-6, 2016.

Samperton, K. M., Schoene, B., Cottle, J. M., Brenhin Keller, C., Crowley, J. L., and Schmitz, M. D.: Magma emplacement, differentiation and cooling in the middle crust: Integrated zircon geochronological–geochemical constraints from the Bergell Intrusion, Central Alps, Chemical Geology, 417, 322–340, https://doi.org/10.1016/j.chemgeo.2015.10.024, 2015.

Samperton, K. M., Bell, E. A., Barboni, M., Keller, C. B., and Schoene, B.: Zircon age-temperature-compositional spectra in plutonic rocks, Geology, 45, 983–986, https://doi.org/10.1130/G38645.1, 2017.

Schaltegger, U., Schmitt, A. K., and Horstwood, M. S. A.: U–Th–Pb zircon geochronology by ID-TIMS, SIMS, and laser ablation ICP-MS: Recipes, interpretations, and opportunities, Chemical Geology, 402, 89–110, https://doi.org/10.1016/j.chemgeo.2015.02.028, 2015.

Schmitt, A., Sliwinski, J., Caricchi, L., Bachmann, O., Riel, N., Kaus, B., Cisneros de Léon, A., Cornet, J., Friedrichs, B., Lovera, O., Sheldrake, T., and Weber, G.: Zircon age spectra to quantify magma evolution, Geosphere, 19, 1006–1031, https://doi.org/10.1130/GES02563.1, 2023.

Schmitt, A. K.: Uranium series accessory crystal dating of magmatic processes, Annual Review of Earth and Planetary Sciences, 39, 321–349, https://doi.org/https://doi.org/10.1146/annurev-earth-040610-133330, 2011.

Schoene, B.: U–Th–Pb Geochronology, in: Treatise on Geochemistry (Second Edition), edited by Holland, H. D. and Turekian, K. K., pp. 341–378, Elsevier, Oxford, https://doi.org/10.1016/B978-0-08-095975-7.00310-7, 2014.

Schoene, B., Schaltegger, U., Brack, P., Latkoczy, C., Stracke, A., and Günther, D.: Rates of magma differentiation and emplacement in a ballooning pluton recorded by U–Pb TIMS-TEA, Adamello batholith, Italy, Earth and Planetary Science Letters, 355-356, 162–173, https://doi.org/10.1016/j.epsl.2012.08.019, 2012.

Siégel, C., Bryan, S., Allen, C., and Gust, D.: Use and abuse of zircon-based thermometers: A critical review and a recommended approach to identify antecrystic zircons, Earth-Science Reviews, 176, 87–116, https://doi.org/10.1016/j.earscirev.2017.08.011, 2018.

Sliwinski, J. T., Guillong, M., Horstwood, M. S. A., and Bachmann, O.: Quantifying long-term reproducibility of zircon reference materials by U-Pb LA-ICP-MS dating, Geostandards and Geoanalytical Research, 46, 401–409, https://doi.org/10.1111/ggr.12442, _eprint: https://onlinelibrary.wiley.com/doi/pdf/10.1111/ggr.12442, 2022.

Sparks, S. R. J., Sigurdsson, H., and Wilson, L.: Magma mixing: a mechanism for triggering acid explosive eruptions, Nature, 267, 315–318, https://doi.org/10.1038/267315a0, 1977.

Szymanowski, D., Ellis, B. S., Wotzlaw, J.-F., and Bachmann, O.: Maturation and rejuvenation of a silicic magma reservoir: High-resolution chronology of the Kneeling Nun Tuff, Earth and Planetary Science Letters, 510, 103–115, https://doi.org/10.1016/j.epsl.2019.01.007, 2019.

Szymanowski, D., Forni, F., Wolff, J. A., and Ellis, B. S.: Modulation of zircon solubility by crystal–melt dynamics, Geology, 48, 798–802, https://doi.org/10.1130/G47405.1, 2020.

Szymanowski, D., Forni, F., Phua, M., Jicha, B., Lee, D. W. J., Hsu, Y.-J., Rifai, H., Schoene, B., and Bouvet de Maisonneuve, C.: A shifty Toba magma reservoir: Improved eruption chronology and petrochronological evidence for lateral growth of a giant magma body, Earth and Planetary Science Letters, 622, 118 408, https://doi.org/10.1016/j.epsl.2023.118408, 2023.

Tavazzani, L., Wotzlaw, J.-F., Economos, R., Sinigoi, S., Demarchi, G., Szymanowski, D., Laurent, O., Bachmann, O., and Chelle-Michou, C.: High-precision zircon age spectra record the dynamics and evolution of large open-system silicic magma reservoirs, Earth and Planetary Science Letters, 623, 118 432, https://doi.org/10.1016/j.epsl.2023.118432, 2023a.

Tavazzani, L., Wotzlaw, J.-F., Economos, R., Szymanowski, D., Laurent, O., Bachmann, O., and Chelle-Michou, C.: AgeSpectraAnalyst: A MATLAB based package to model zircon age distributions in silicic magmatic systems, MethodsX, 11, 102 406, https://doi.org/10.1016/j.mex.2023.102406, 2023b.

Tierney, C. R., Schmitt, A. K., Lovera, O. M., and de Silva, S. L.: Voluminous plutonism during volcanic quiescence revealed by thermochemical modeling of zircon, Geology, 44, 683–686, https://doi.org/10.1130/G37968.1, 2016.

Vermeesch, P.: On the visualisation of detrital age distributions, Chemical Geology, 312-313, 190–194, https://doi.org/10.1016/j.chemgeo.2012.04.021, 2012.

Vermeesch, P.: Multi-sample comparison of detrital age distributions, Chemical Geology, 341, 140–146, https://doi.org/10.1016/j.chemgeo.2013.01.010, 2013.

Virmond, A. L., Wotzlaw, J.-F., Rojas-Arrancibia, R., Selby, D., and Chelle-Michou, C.: Multi-million-year magmatic and hydrothermal activity is key to the formation of supergiant to behemothian porphyry copper deposits, Contributions to Mineralogy and Petrology, 179, 88, https://doi.org/10.1007/s00410-024-02167-4, 2024.

Watson, E. B.: Dissolution, growth and survival of zircons during crustal fusion: kinetic principals, geological models and implications for isotopic inheritance, Earth and Environmental Science Transactions of The Royal Society of Edinburgh, 87, 43–56, https://doi.org/10.1017/S0263593300006465, 1996.

Weber, G., Caricchi, L., Arce, J. L., and Schmitt, A. K.: Determining the current size and state of subvolcanic magma reservoirs, Nature Communications, 11, 5477, https://doi.org/10.1038/s41467-020-19084-2, 2020.

Widmann, P., Davies, J. H. F. L., and Schaltegger, U.: Calibrating chemical abrasion: Its effects on zircon crystal structure, chemical composition and U–Pb age, Chemical Geology, 511, 1–10, https://doi.org/10.1016/j.chemgeo.2019.02.026, 2019.

Wotzlaw, J.-F., Schaltegger, U., Frick, D. A., Dungan, M. A., Gerdes, A., and Günther, D.: Tracking the evolution of large-volume silicic magma reservoirs from assembly to supereruption, Geology, 41, 867–870, https://doi.org/10.1130/G34366.1, 2013.

Wotzlaw, J.-F., Bindeman, I. N., Stern, R. A., D'Abzac, F.-X., and Schaltegger, U.: Rapid heterogeneous assembly of multiple magma reservoirs prior to Yellowstone supereruptions, Scientific Reports, 5, 14 026, https://doi.org/10.1038/srep14026, 2015.